

Oriental superlattices formed by CuPt-ordered zinc-blende semiconductor alloys

Yong Zhang and A. Mascarenhas

National Renewable Energy Laboratory, Golden, Colorado 80401

(Received 21 August 1996; revised manuscript received 15 October 1996)

We performed a systematic study on a nonconventional semiconductor heterostructure—*orientational superlattices* (OSL's)—based on CuPt-ordered zinc-blende alloys. Instead of the band offset in conventional superlattices, it is the discontinuity in the angular momentum which brings about the superlattice effects in orientational superlattices. Valence-band structures of five polytypes of OSL's formed by CuPt-ordered GaInP₂ layers have been classified according to their symmetries and calculated numerically by using the envelope-function approximation for structures with different periods, ratios of layer thickness, and degree of order. On one hand, features similar to those in conventional superlattices—wave-function modulation, band-gap modification, and the formation of subbands and minigaps—can be achieved purely from an orientational alternation of the semiconductor layers. On the other hand, the dependence of energy levels on layer thickness and the wave-function distributions in OSL's are distinct from that in conventional superlattices.

[S0163-1829(97)04319-1]

I. INTRODUCTION

Esaki and Tsu¹ proposed the concept of a semiconductor superlattice (SL) in which electrons (holes) are confined by a one-dimensional scalar potential generated by alternating the doping with donors and acceptors or varying alloy composition in thin semiconductor layers. In the Esaki-Tsu-type superlattices, quantum confinement is most often achieved by the band-gap difference between two semiconductors. In the envelope-function approximation,² the effective Hamiltonian for electronic states usually has an effective potential in the form of a diagonal matrix. The matrix elements are given by the band offsets between adjacent semiconductor layers. Other than the band offsets, the discontinuity of the effective-mass tensor varying from one layer to the other also plays a role in determining the electronic states.² There are certain situations in which the spatial confinement for electrons and holes can be understood as caused by the spatial variation of the effective-mass tensor. For instance, (GaP₂/InP)₂ bilayer SL with lateral composition-modulation (the so-called spontaneously generated effective-mass lateral SL's) is one such situation.³ However, this type of effective-mass SL can as well be treated as a problem with a uniform effective-mass tensor and an effective potential having off-diagonal matrix elements, which is a tensorlike effective potential.^{4,5} Thus, in this type of effective-mass superlattice, the quantum confinement is still associated with the spatial variation of the band gap or a continuously varying band offset. In short, most of the previously studied semiconductor SL's can be considered as generalized Esaki-Tsu SL's in which symmetric axes of the alternating layers are aligned in parallel and so the "effective potential" matrices have the same form, but the values of the matrix elements vary spatially. Band-gap differences always exist between the two constituents. We refer to this type of superlattice as a *conventional superlattice*.

Another type of superlattice is the *orientational superlattice* (OSL). In an OSL, by definition, when going from one constituent to the other, neither the magnitude nor the symmetry of the lattice potential is changed, but the symmetry

axis is rotated periodically. Silicon carbide (SiC) polytypes are good examples of this type of superlattice. As pointed out by Backes, Bobbert, and van Haeringen,⁶ SiC polytypes may be viewed as natural superlattices consisting of pure 3C SiC segments that differ in size and crystallographic orientation only. Usually, in these superlattices each segment contains only a few monolayers of the 3C structure. Another example of the orientational superlattices is the so-called "twinning superlattices"⁷ which is hypothetically formed by arranging twin stacking faults in a periodic sequence. Besides semiconductors, OSL's have also been found in metals (a periodic antiphase boundary structure of ordered CuAu,⁸ for instance).

Recently, a different category of OSL-like structure was observed in CuPt-ordered III-V semiconductor alloys.^{9,10} It has been well established that by using the growth technique of metal-organic vapor-phase epitaxy, various III-V alloys $A_{1-x}B_xC$ ($x \sim 0.5$) can spontaneously form a monolayer superlattice AC/BC along either one of the two $[111]_B$ directions.¹¹ Depending on the orientation of the substrates, one can obtain ordered alloys with single- or double-ordering variants. A single-variant ordered alloy shows the symmetry of a CuPt structure, as compared to the zinc-blende symmetry of the disordered alloy. Band-gap reduction, valence-band splitting, and changes in optical polarization are the major features of the ordering, and these features have been well studied.¹¹ On the other hand, ordered alloys with double-variant structures have received much less attention, and researchers often try to suppress the second variant by growing the epilayers on tilted substrates. We have pointed out¹² that a category of OSL's can be constructed from double-variant-ordered structures. In fact, spatial alternation in the direction of the ordering axis has been observed in double-variant-ordered Ga_xIn_{1-x}P alloys: periodic structures of domain boundaries between the two variants appear either along the $[001]$ growth direction^{9,10} or along the $[\bar{1}11]$ direction¹³ (where we define the $[111]$ and $[\bar{1}11]$ as the ordering direction for the two variants). The $[001]$ structures are found to have a periodicity of about 10 nm, and the $[\bar{1}11]$ structures have a large periodicity of the order of 1 μm . The

[110] structures have also been achieved by growing $\text{Ga}_x\text{In}_{1-x}\text{P}$ epilayers on patterned substrates.¹⁴ Although the periodicities in the above-mentioned structures are far less than perfect, they demonstrate the feasibility of growing semiconductor OSL's epitaxially. The double-variant structures reported in Refs. 9, 10 have also been obtained in our laboratory. Moreover, the change in optical properties (e.g., enhancement of optical anisotropy) as compared to those in single-variant structures has been observed experimentally,¹⁵ as should be expected for the OSL's whose band structures will be studied in this work.

Band structures of certain SiC polytypes have been calculated successfully by using the superlattice approach.⁶ This assumption is comparable to the flat-band approximation in the description of conventional superlattices in which the layers are assumed to be entirely bulklike.² Conduction-band structures for Si, Ge, AlAs, and GaAs twinning superlattices have been calculated by using a microscopic technique (empirical-pseudopotential-based layer technique).⁷ The superlattice effects—the change of band-edge energy and the formation of minibands—are found very prominently in indirect-gap materials and short-period (less than 10 ML) structures. For direct-gap semiconductors and long-period structures, the superlattice effect is merely a small shift in band-edge energy, which is essentially because the s -like Γ conduction state is not sensitive to the rotation of the crystal potential. For valence bands, the superlattice effects are negligibly weak.¹⁶ The authors of Ref. 7 also pointed out that many of the effects in twinning superlattices cannot be understood within the “continuum” models, such as the effective-mass method, because neither the potential nor the effective-mass change across the boundary. As will be discussed later, this statement is not generally valid for OSL's, although it is valid for the special cases in which OSL's are constructed from their parent lattices that have diamond or zinc-blende symmetry. For OSL's formed by ordered alloys like $\text{Ga}_x\text{In}_{1-x}\text{P}$, because of its direct band gap, one would not expect strong changes to the conduction-band electronic structure unless very short-period structures are considered. However, for the valence band, because of its p -like symmetry, one could expect that the rotation of the uniaxial axis of the ordered crystal will bring about changes in the valence-band structure. We recently investigated the band structure of the valence bands for OSL's based on ordered $\text{Ga}_x\text{In}_{1-x}\text{P}$ alloys.¹² The purpose of this work is to give a systematic description of the band structure for different polytypes of OSL's formed by ordered zinc-blende alloys and to discuss the differences between conventional and orientational superlattices. The same “flat-band approximation” used for conventional superlattices² and for orientational superlattices of SiC polytypes⁶ is applied, and the envelope-function method² is used in this work. Analogous to conventional superlattices, these orientational superlattices also show spatially varying amplitudes of the envelope functions, modifications to the band-edge states and band gaps, and the appearance of subbands and miniband gaps, but often in different or complementary ways. Characteristic features of five distinct polytype structures are discussed in relation to their symmetry.

This paper is organized as follows: Section I is an Introduction. In Sec. II, we describe five of the simplest possible

OSL structures formed by CuPt-ordered GaInP_2 , construct superlattice potentials for the five polytype OSL's, discuss the difference in superlattice potentials for conventional and orientational superlattices, and, using an envelope-function approximation, calculate energy dispersions and probability distributions for the five polytypes. Section III discusses certain distinct properties of OSL's, as well as the approximations and the limitations of our theoretical approach to modeling these structures. Section IV summarizes this work.

II. MODEL AND CALCULATIONS

A. Structures of polytypes

Figure 1 shows five types of the most simple OSL structures based on ordered CuPt alloys. These structures could be grown artificially or formed spontaneously. They consist of two differently oriented layers in a single superlattice period. One layer is related to the other one by a rotational operation R of the point group T_d : 180° rotation about the [001] axis for types I, III, and IV; 240° rotation about the [111] axis for types II and V. The arrows in Fig. 1 are to be understood as directions pointing from Ga-rich to In-rich layers (or the other way). The relative arrow directions shown in the Fig. 1 represent OSL structures without antiphase boundaries.¹⁷ The difference among types I, III, and IV or between types II and V is in the stacking direction. For types I, III, and IV, the ordering directions of the two layers are in the same plane, but this is not so for types II and V.

If the atomic arrangements at the interface are taken into account, for each polytype in Fig. 1, there are three microscopically distinct structures. The reversal in the direction of one of the arrows in each polytype is associated with the occurrence of a zinc-blende or CuPt antiphase boundary at the interface of the two variants. A zinc-blende antiphase boundary can be generated by combining the rotation R with a translation T' that does not belong to the space group ($F\bar{4}3m$) of the zinc-blende crystals (it interchanges cation planes with anion planes). For any one of the structures shown in Fig. 1, this procedure gives a new structure microscopically different from the original one. Another distinct structure can be obtained by combining the rotation R with a translation T that interchanges the Ga and In cation planes and generates a CuPt antiphase boundary. T belongs to $F\bar{4}3m$ but not to $R3m$ (the space group of the CuPt structure). In this work, we try to focus on the bulk effects of the OSL. To avoid the complexity of the interfaces, we limit the situation to that in which the layer thickness is much larger than that of a monolayer, and assume that in this limit the interface effects are negligible. This is a valid assumption for the conventional superlattice, but has not yet been rigorously investigated for OSL's (this issue will be addressed later in Sec. IV). Therefore, we do not distinguish the structures shown in Fig. 1 from the other structures associated with the occurrence of antiphase boundaries generated by T' or T , and the arrows in Fig. 1 can be removed.

Note that polytypes I and III, consisting of [111]- and $[\bar{1}\bar{1}\bar{1}]$ -ordered variants alternatively stacked along the [100] or [110] directions, are the double-variant structures observed experimentally by Refs. 9, 10, 15 and Refs. 13, 14, respectively. Type IV can be viewed as the same double-

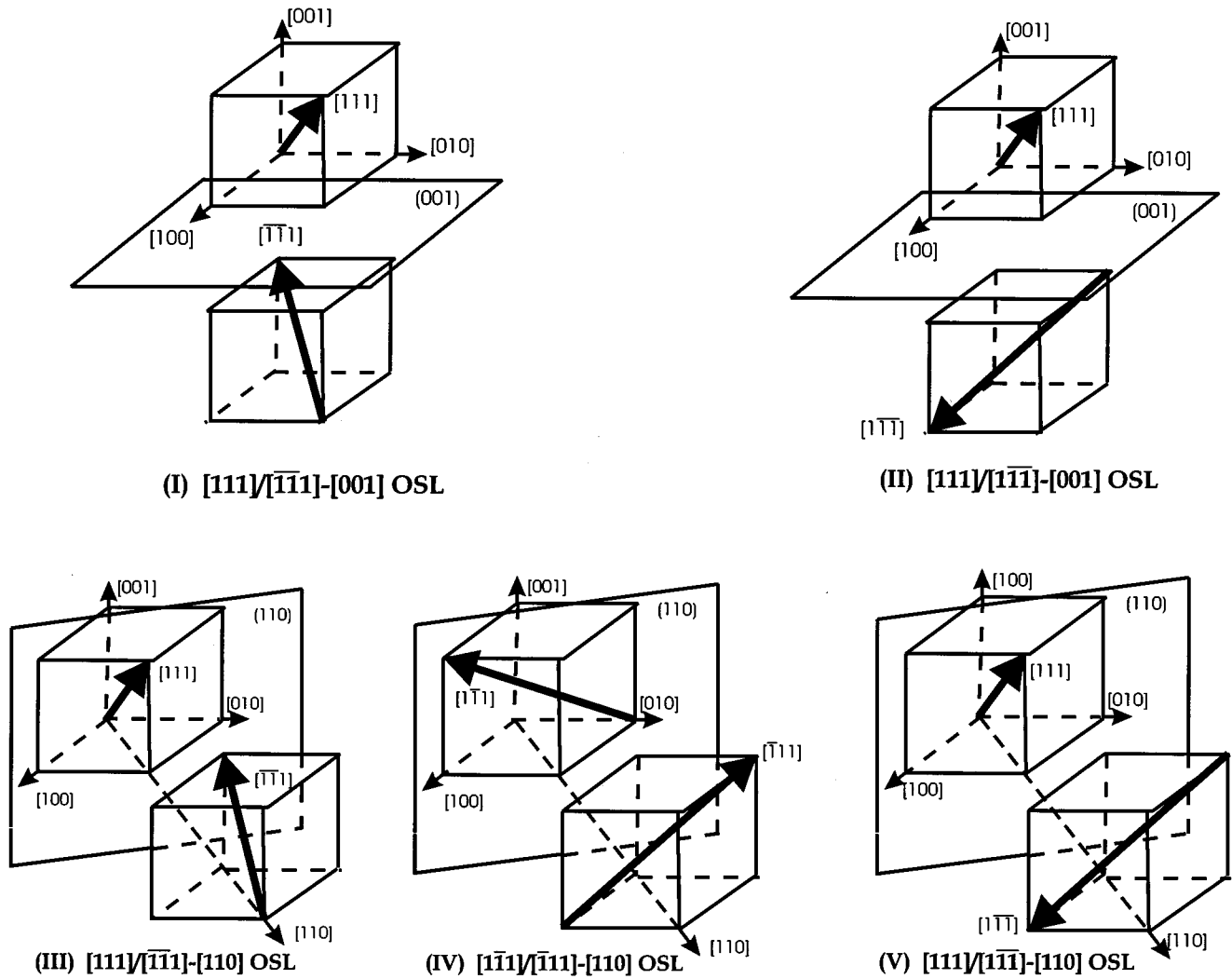


FIG. 1. Five polytype orientational superlattices based on CuPt-ordered GaInP₂ alloys. The relative arrow directions represent the structures without antiphase boundaries.

variant structure but stacked along the $[110]$ direction. This polytype is similar to twinning superlattices,⁷ because one variant is twisted by an angle of $\cos^{-1}(1/3)$ with respect to the other about the superlattice axis. Higher-index polytypes (for instance, structures with three or more differently oriented layers in one period) are not considered in this work. The symbol $[111]/[\bar{1}\bar{1}\bar{1}]-[110]$ represents an OSL with layers alternately ordered along the $[111]$ and $[\bar{1}\bar{1}\bar{1}]$ directions, and the superlattice axis along the $[110]$ direction.

B. Superlattice potentials

If a superlattice contains two different layers (A and B) in one period, the superlattice potential can be written as $\Delta V(\mathbf{x}) = V_B(\mathbf{x}) - V_A(\mathbf{x})$ in layer B and $\Delta V(\mathbf{x}) = 0$ in layer A , where $V_A(\mathbf{x})$ and $V_B(\mathbf{x})$ are the periodic potentials in the bulk materials A and B , respectively. If layer A is taken as the reference, to a first-order approximation, the superlattice potential in layer B becomes $\Delta V = \langle U_A | \Delta V(\mathbf{x}) | U_A \rangle$, where U_A is the band-edge Bloch state of the layer A . For a conventional superlattice, with the assumption of $U_A = U_B$,² ΔV is then the band offset between layers A and B . This

assumption implies that the potentials in layers A and B have the same functional form and differ only in their strength. The band gaps—and so the effective masses—are different in layers A and B . For an orientational superlattice, by definition, $V_B(\mathbf{x}) = R^{-1}V_A(\mathbf{x})R$, where R is a rotational operator that does not belong to the symmetry group of the host crystal. In the twinning superlattice studied by Ref. 7, the layer B is related to layer A by a 180° rotation about the $[111]$ axis. Even though the rotation does not belong to the symmetry operation of the T_d group, to the first-order approximation, the twinning superlattice has no effect on the valence-band states with wave vector \mathbf{k} along the superlattice axis, because the unperturbed band-edge states are p like. Thus, the twinning superlattice is a higher-order effect which needs the coupling among states with the \mathbf{k} vector near and away from the Brillouin-zone center or states inside and outside the eight-band manifold.

We are going to show that for OSL's constructed by epilayers with uniaxial symmetry, superlattice effects, such as band-gap changes, wave-function modifications, and mini-gaps, appear in the first-order treatment of the valence-band states, even in the absence of band offsets and effective-mass

discontinuities. The potential for a single-variant ordered alloy can be written as $V(\mathbf{x})=V_0(\mathbf{x})+\delta V(\mathbf{x})$, where $V_0(\mathbf{x})$ is the potential for the disordered alloy in the ‘‘virtual-crystal approximation,’’ $\delta V(\mathbf{x})$ is the perturbation due to ordering. For the valence bands (VB’s), the effective Hamiltonian for the perturbation can be written in a way similar to that for an [111]-uniaxial strain,^{18–21,12}

$$h = -d[(L_x L_y + L_y L_x)\varepsilon_{xy} + \text{c.p.}], \quad (1)$$

where \mathbf{L} is the orbital angular momentum, and c.p. denotes cyclic permutation with respect to the indices x , y , and z . Parameter d describes the strength of the rhombohedral distortion, and the tensor ε describes the ordering direction. For

$i \neq j$, $\varepsilon_{ij} = \pm 1$, depending on the ordering direction (for instance, $\varepsilon_{xy} = 1$ for [111] ordering, $\varepsilon_{xy} = -1$ for $[\bar{1}\bar{1}\bar{1}]$ ordering and so on); for $i = j$, $\varepsilon_{ij} = 0$. The coordinate axes x , y , and z have been chosen along the [100], [010], and [001] directions, respectively. By using the three p -like band-edge states ($|X\rangle$, $|Y\rangle$, and $|Z\rangle$) of the disordered alloy as a basis, the matrix form of Eq. (1) is

$$h = d \begin{pmatrix} 0 & \varepsilon_{xy} & \varepsilon_{xz} \\ \varepsilon_{xy} & 0 & \varepsilon_{yz} \\ \varepsilon_{xz} & \varepsilon_{yz} & 0 \end{pmatrix}, \quad (2)$$

and with spin-orbit interaction included, Eq. (1) becomes

$$h = \begin{pmatrix} 0 & s^* & r^* & 0 & -\frac{1}{\sqrt{2}}s^* & \sqrt{2}r^* \\ s & 0 & 0 & -r^* & 0 & \sqrt{\frac{3}{2}}s^* \\ r & 0 & 0 & s^* & -\sqrt{\frac{3}{2}}s & 0 \\ 0 & -r & s & 0 & -\sqrt{2}r & -\frac{1}{\sqrt{2}}s \\ -\frac{1}{\sqrt{2}}s & 0 & -\sqrt{\frac{3}{2}}s^* & -\sqrt{2}r^* & 0 & 0 \\ \sqrt{2}r & \sqrt{\frac{3}{2}}s & 0 & -\frac{1}{\sqrt{2}}s^* & 0 & 0 \end{pmatrix}, \quad (3)$$

with $r = -id\varepsilon_{xy}/\sqrt{3}$, $s = -d(\varepsilon_{xz} - i\varepsilon_{yz})/\sqrt{3}$. The basis for Eq. (3) is the same as what is normally used for a cubic crystal: $\{|J, m_z\rangle\} = \{|3/2, -3/2\rangle, |3/2, -1/2\rangle, |3/2, 1/2\rangle, |3/2, 3/2\rangle, |1/2, -1/2\rangle, |1/2, 1/2\rangle\}$, where $\mathbf{J} = \mathbf{L} + \mathbf{S}$, \mathbf{S} and \mathbf{J} are the spin and total angular momentum, respectively. When using Eq. (1) to describe the ordering effect, we have ignored the small change in spin-orbit interaction due to ordering.^{11,21}

Assuming the superlattice axis is along the z' direction and $z' = 0$ is at the center of layer A , the superlattice potential is then

$$\Delta h(z') = [h_B - h_A]\theta(z'), \quad (4)$$

where h_A and h_B are given by Eq. (3) in layer A (with thickness L_A) and layer B (with thickness L_B), respectively. $\theta(z') = 0$ when z' is in the layer A , and $\theta(z') = 1$ when z' is in the layer B . We assume layer A and layer B have the same degree of order, so we can study the effects purely due to the orientational change [the eigenvalues of Eq. (3) are the same in layer A and layer B : therefore, there are no band offsets for band-edge states]. The conduction band and valence band have been decoupled because of the relatively large band gap ($E_g \sim 2$ eV). Because the anisotropy of the conduction band is mainly due to its coupling to the well-separated valence

band, we expect that the OSL effects are weak for the conduction band.²² Thus, we will focus only on the valence band. We would like to point out that because the spin-orbit interaction is not involved in the perturbative Hamiltonian, the spin-orbit interaction does not directly contribute to the OSL effects, but does so indirectly through the zinc-blende Hamiltonian, H_{dis} , defined below.

C. Energy dispersion and probability distribution

Recently, we have calculated the band structure of single-variant or ‘‘bulk’’ ordered GaInP₂ using an eight-band $\mathbf{k}\cdot\mathbf{p}$ model,²¹ where the ordering direction was defined as the [111] direction. For a bulk CuPt-ordered III-V alloy, the VB effective Hamiltonian can be written as

$$H_{\text{ord}} = H_{\text{dis}} + h, \quad (5)$$

where H_{dis} is the six-band $\mathbf{k}\cdot\mathbf{p}$ Hamiltonian for the disordered alloy and given by Eq. (A6) of Ref. 21. In H_{dis} , terms related to the lack of inversion symmetry in zinc-blende crystals are ignored, since their effects are usually very weak.² As for conventional SL’s, the OSL’s can be treated in the envelope-function approximation.² Note that the superlattice potential Eq. (4) is a tensor with all the diagonal terms

TABLE I. Band-structure parameters for the disordered GaInP₂ alloy.

E_g (eV)	Δ (meV)	E_p (eV)	m_0^* (m_e)	γ_1	γ_2	γ_3
1.991	103	26	0.092	4.55	1.05	1.49

being zero in the coordinate system (x, y, z) . One could also treat this type of OSL as an effective-mass OSL for which the principal axes of the effective-mass tensor (or, more generally, energy-dispersion functions) have different orientations in the adjacent layers. However, this is inconvenient because the dispersions are strongly nonparabolic.²¹

The eigenvalue equation for the OSL is then

$$[H_0 + \Delta h(z')] \mathbf{F} = \mathbf{E} \mathbf{F}, \quad (6)$$

where $H_0 = H_{\text{dis}}(\mathbf{k}_{z'} \rightarrow -i\nabla_{z'}) + h_A$ is the Hamiltonian for the bulk-ordered GaInP₂, and $\mathbf{F} = (f_1, f_2, \dots, f_6)$ are six-band envelope functions. Note that H_0 is given in the coordinate system (x, y, z) as a function of wave vector $\mathbf{k} = (k_x, k_y, k_z)$. When the superlattice axis is not along the [001] direction, we transform H_0 to the coordinate system (x', y', z') , in which H_0 becomes a function of the wave vector $\mathbf{q} = (q_1, q_2, q_3)$, with q_3 along the superlattice axis and q_2 and q_3 in the plane perpendicular to the superlattice axis. However, we do not change the basis of the six-band manifold.

A Fourier transform method^{23,24} is used to solve the eigenvalue problem of Eq. (6), with a periodic boundary condition $\mathbf{F}(z') = \mathbf{F}(z' + L_A + L_B)$ implied. The validity of this boundary condition will be discussed later. The envelope functions can be expanded in a Fourier series,

$$f_j(\mathbf{q}; z') = \sum_{n=-m}^m b_{jn}(\mathbf{q}) \exp(inK_0 z'), \quad (7)$$

where $K_0 = 2\pi/(L_A + L_B)$, and m is a finite number, depending on the accuracy required. The solution of Eq. (6) involves obtaining the eigenvalues and eigenvectors of a $6(2m+1) \times 6(2m+1)$ matrix. The wave functions of the electronic states are given as

$$\varphi_{\mathbf{q}}(\mathbf{x}') = \exp(i\mathbf{q} \cdot \mathbf{x}') \sum_{j=1}^6 f_j(\mathbf{q}, z') u_{0j}, \quad (8)$$

where u_{0j} are band-edge states of the disordered alloy.

The corresponding probability distribution is defined as²⁵

$$p(z') = \sum_{j=1}^6 |f_j(z')|^2, \quad (9)$$

where the normalization condition is $\int_{L_A + L_B} p(z') dz' = L_A + L_B$. Note that $\sum_{j=1}^6 |f_j(\mathbf{q})|^2 = 1$ for a bulk-ordered alloy.

For numerical calculations, we use a typical value of $d = -15$ meV, which corresponds to a heavy-light-hole splitting of 25 meV and a band-gap reduction of 106 meV in a single-variant-ordered GaInP₂.^{21,26} This value of d represents the situation for the strongest ordered samples currently achieved experimentally.²⁶ The band structure parameters for disordered GaInP₂ are listed in Table I.

TABLE II. Band-edge energy differences between the top of VB in ordered GaInP₂ and the five polytype OSL's of GaInP₂, compared with the projection of the orientational tensor ε in the superlattice axes.

	I	II	III	IV	V
$\delta E = E_{\text{ord}} - E_{\text{OSL}}$ (meV)	2.46	2.47	3.22	1.71	2.12
$\frac{1}{2} (\varepsilon_A \cdot \mathbf{u} + \varepsilon_B \cdot \mathbf{u})$	$\sqrt{2}$	$\sqrt{2}$	$\sqrt{3}$	1	$\frac{(1+\sqrt{3})}{2}$

First, we consider symmetric superlattices for which layers A and B are of equal thickness. Table II shows the energy shift δE (the energy of the top of the VB with respect to that of the top of the VB in a bulk-ordered GaInP₂ alloy) for the five types of GaInP₂ OSL's with $L_A = L_B = 100$ Å. The shift of the VB maximum in OSL's is similar to that in conventional SL's; that is, the shift tends to increase the band gap from the bulk value. This energy shift, referred to as ‘‘confinement energy’’ in conventional SL's, is largest in type III, intermediate in types I, II, and V, almost the same in types I and II, and smallest in the type-IV structures, as summarized in Table II. Figures 2(a) and 2(b) show the dispersion curves $E(q_3)$ for types I and V, respectively. The results for types II–IV are qualitatively similar to that of type I. For these four polytypes, two adjacent subbands meet at the zone boundary ($q_3 = 0.5K_0$) i.e., the folded bands are degenerate at the zone boundary. Also shown in Fig. 2(a) as dashed curves are the folded bands of bulk-ordered GaInP₂ in the [001] dispersions. Type V, as shown in Fig. 2(b), is distinct from the other four polytypes: a mini-band-gap opens at the zone boundary. Note that type V is not a pure orientational superlattice. With respect to the superlattice axis, layers A and B are equivalent for all the polytypes except for type V. In type V, the ordering direction of the layer A is coplanar with the superlattice axis and that of the layer B is not. Thus, the energy dispersions in the two layers are different along the superlattice axis even without considering any superlattice effects, which indicates that there is a band offset between the two layers for $\mathbf{q} \neq \mathbf{0}$. This situation is similar to most conventional superlattices, in which the band offset and the effective-mass discontinuity coexist, but here there is a coexistence of the orientational discontinuity and effective-mass discontinuity.

Let us now study the spatial probability distribution of valence-band states in OSL's. For types I-IV, because layers A and B are equivalent with respect to the superlattice axis, we expect to see an identical probability distribution in the two layers. For type V, however, we expect that the envelope function will be more confined in the layer with heavier mass (or lower energy when going away from $\mathbf{q} = \mathbf{0}$), because the superlattice potential mixes Bloch states near $\mathbf{q} = \mathbf{0}$, and there are band offsets for $\mathbf{q} \neq \mathbf{0}$ states. More specifically, the ground-state envelope-function will localize in the layer for which the ordering direction is coplanar with the superlattice axis because the effective mass in the [110] direction is heavier than that in the $\bar{[110]}$ direction.²¹ Figures 3(a) and 3(b) show the probability distributions of the band-edge states of the first four subbands for types I and V, respectively. The results of types II-IV are similar to that of type I.

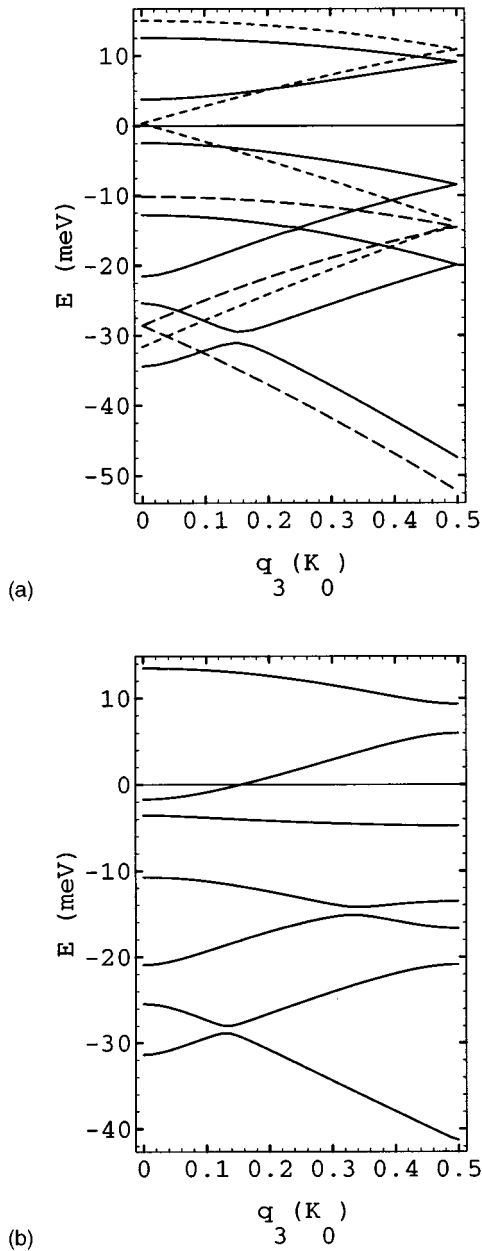


FIG. 2. Energy-dispersion curves $E(q_3)$ of symmetric OSL's with $L_A=L_B=100 \text{ \AA}$ along the superlattice axes: (a) type I and (b) type V. Dashed curves in (a) are the folded bands of the bulk-ordered alloy.

For types I-IV, no confinement in an individual layer is expected, but spatial modulation of the envelope function appears for these OSL's. The envelope functions maximize at the centers of the two layers for the first, second, and fourth states and at the interfaces of the two layers for the third state. An especially interesting point is that the third state has zero probability at the centers of the layers. The probability distributions of these OSL's are somewhat similar to conventional superlattices with thin barriers. For the OSL structures, the interface acts like the barriers. For type V, the probability distributions are unequal for the two layers or ordered domains. For the ground state, referred to as the type-V structure shown in Fig. 1, the envelope function is mostly localized in the [111]-ordered layer. For the third state, the

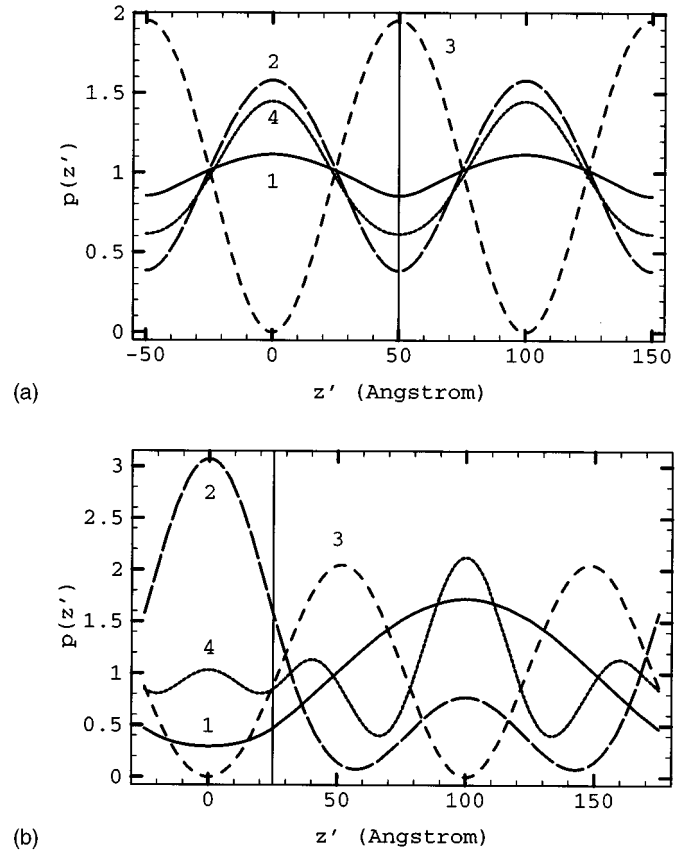


FIG. 3. Probability distributions of the first four band-edge states (labeled as 1-4) of symmetric OSL's with $L_A=L_B=100 \text{ \AA}$: (a) type I and (b) type V.

envelope function is still zero at the center of each layer, but the maximum position shifts toward the [111]-ordered layer.

Second, we consider the asymmetric OSL structures. For $L_A=50 \text{ \AA}$ and $L_B=150 \text{ \AA}$, Figs. 4(a) and 4(b) are dispersion curves of $E(q_3)$'s for types I and type V, respectively. The results shown in Fig. 4(a) are typical for types I-IV. In all these asymmetric structures, the degeneracy at the zone boundary has been removed and mini-band-gaps appear, as opposed to being observed only for type V in the symmetric case. The appearance of the mini-band-gaps is obviously associated with the lack of rotational symmetry R .

Except for type V, the confinement energy of an asymmetric OSL is smaller than that of a symmetric one of the same type—that is, the confinement energy maximizes at the ratio $L_A/L_B=1$. Figure 5 shows the confinement energy as a function of the superlattice period L_A+L_B with different L_A/L_B ratios for type-III structures. For type V, the confinement energy first increases when reducing the thickness (L_A) of the layer in which the envelope function is localized for the symmetric case. After reaching a maximum at a value of $L_A/L_B < 1$, the confinement energy starts to decrease. On the other hand, increasing the superlattice period L_A+L_B decreases the confinement energy just as for all the other types. Figure 6 shows the confinement energy as a function of ratio L_A/L_B for different values of L_A+L_B . For a conventional SL, one expects that the confinement energy increases when reducing the well width, until the well width approaches a certain value at which the increase stops be-

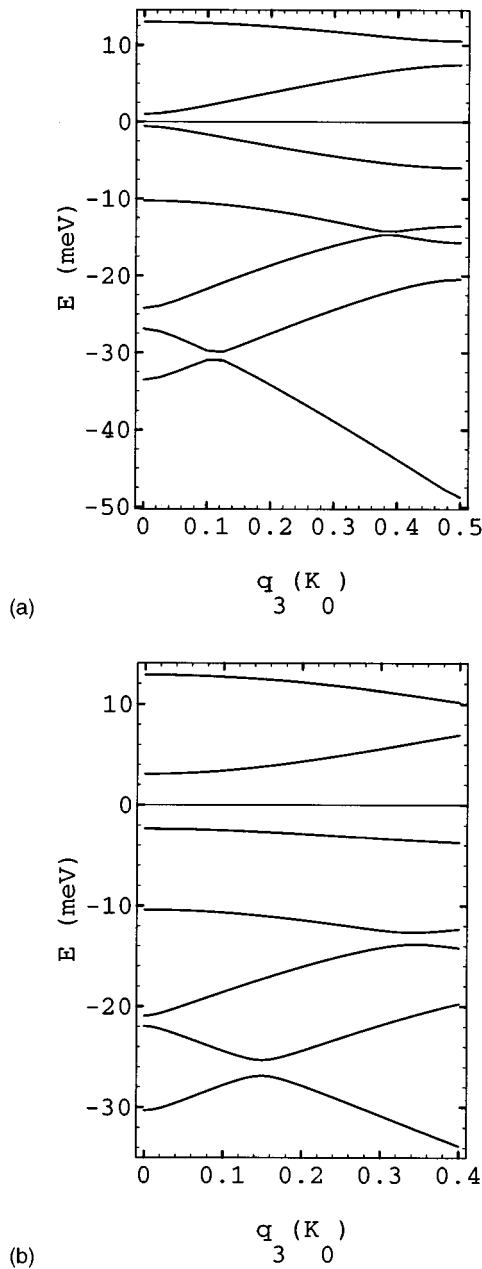


FIG. 4. Energy-dispersion curves $E(q_3)$ of asymmetric OSL's with $L_A = 50 \text{ \AA}$ and $L_B = 150 \text{ \AA}$ along the superlattice axes: (a) type I and (b) type V.

cause of the wave function leakage into the barriers. What happens in the type-V OSL is similar to that in a conventional SL.

Figures 7(a) and 7(b) are the probability distributions of the valence-band states for the asymmetric OSL's of types I and V, corresponding to Fig. 4. For all the five types, the probability distributions are qualitatively the same: the ground states are more localized in the wider layer, the second states in the narrower layer, the third states near the interface but in the wider layer, the fourth states in the wider layer, etc.

Next, we consider the energy dispersions with wave vectors in the plane perpendicular to the superlattice direction. As an example, Fig. 8 shows the results for the type-I structure with $L_A = L_B = 100 \text{ \AA}$ [Figs. 8(a) and 8(b)] and $L_A = 50 \text{ \AA}/L_B = 100 \text{ \AA}$ [Figs. 8(c) and 8(d)] for \mathbf{k} along the

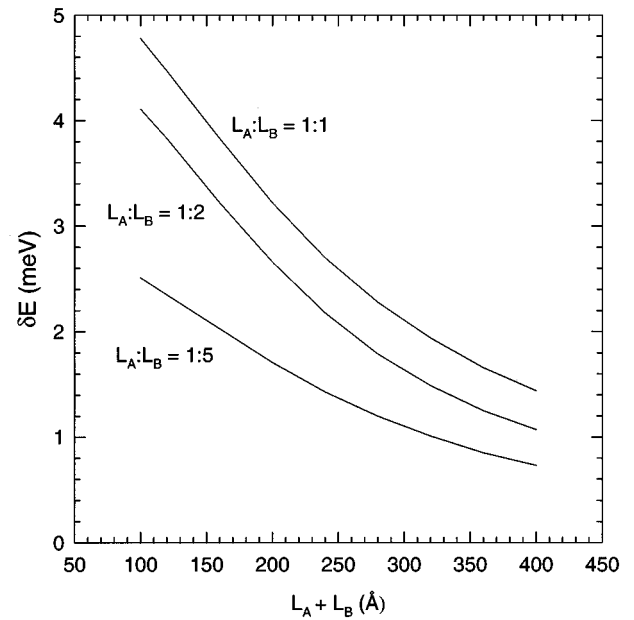


FIG. 5. Confinement energy, δE , of the first subband as a function of superlattice period $L_A + L_B$ for type-III SL's at various L_A/L_B ratios.

$[110]$ and $[\bar{1}\bar{1}0]$ directions, respectively, with comparison to the in-plane dispersions of the bulk-ordered structure. In general, the energy dispersion is anisotropic for \mathbf{k} in the plane perpendicular to the superlattice direction, which is correlated with the property $m_{[110]} > m_{[\bar{1}\bar{1}0]}$ of the bulk-ordered alloy. For the first subbands, the effective masses become slightly heavier than that of the bulk-ordered alloy. On the other hand, some subbands have very heavy effective masses or nearly flat dispersion curves near $\mathbf{k} = \mathbf{0}$. Away from the zone center, dispersion curves become more similar to that of the bulk-ordered alloy (shown by the dashed lines). For

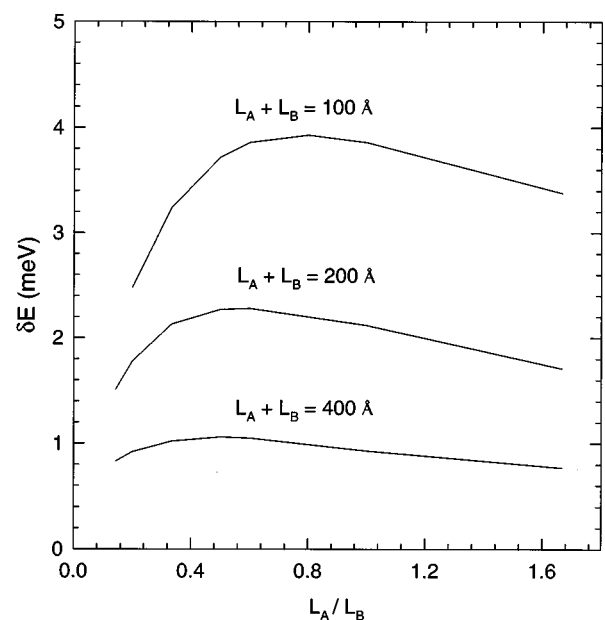


FIG. 6. Confinement energy, δE , of the first subband as a function of L_A/L_B ratio for type-V SL's at various superlattice periods $L_A + L_B$.

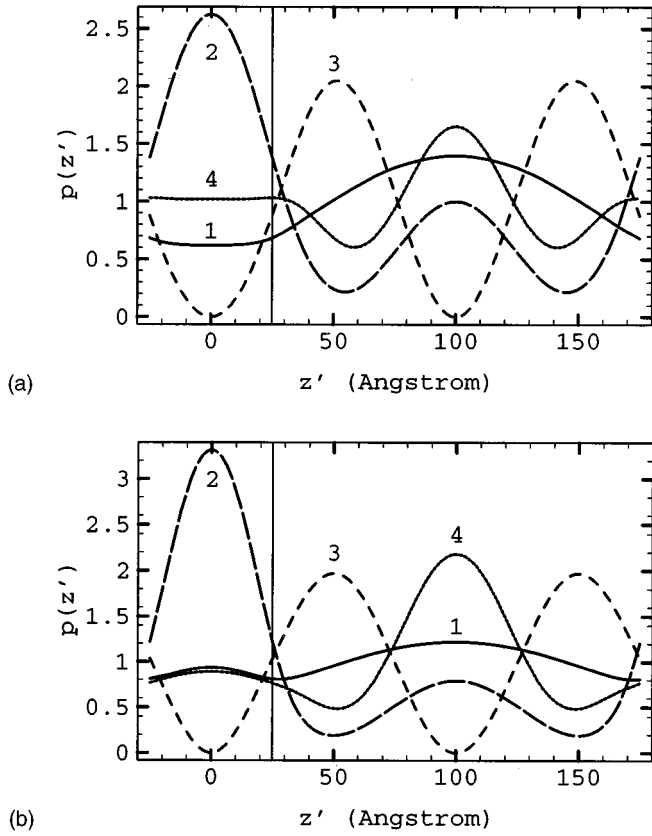


FIG. 7. Probability distributions of the first four band-edge states (labeled as 1–4) of asymmetric OSL's with $L_A=50 \text{ \AA}$ and $L_B=150 \text{ \AA}$: (a) type I and (b) type V.

the symmetric structure, Figs. 8(a) and 8(b), when \mathbf{k} is in the $[110]$ direction which is coplanar with the ordering direction, every two subbands merge into one at large \mathbf{k} ; when \mathbf{k} is in the $[1\bar{1}0]$ direction, subbands do not merge together but become parallel. For the asymmetric structure, Figs. 8(c) and 8(d), subbands do not merge in either the $[110]$ or the $[1\bar{1}0]$ directions.

Finally, we consider the dependence of the OSL effects on the degree of order. Figure 9 shows the energy levels of the first and the second band-edge states as a function of parameter $|d|$ for types-I and -III OSL's with $L_A=L_B=50 \text{ \AA}$, with a comparison to those of bulk-ordered alloy. As one can see, the confinement energy $\delta E = E_{\text{ord}} - E_{\text{OSL}}$ increases with increasing degree of order. An important character of OSL's is that, while in the bulk case the topmost VB state has a linear $|d|$ dependence, the dependence becomes nonlinear due to the interaction with other subbands, which suggests that the band gap will not have a linear $|d|$ dependence any more. Another important feature is that the splitting of the first two VB states is significantly smaller than that of the bulk-ordered alloy for the same degree of order.

III. DISCUSSION

A. Approximations and limitations of our model calculations

The aim of this work is to present properties of orientational superlattices. A greatly simplified model has been employed in our calculations. The major approximations made

are (1) the OSL's are treated in the subspace of $\Gamma_8 \otimes \Gamma_7$ of the zinc-blende structure; (2) the interface effects have been ignored.

It has been well demonstrated that Eq. (1) can describe very well certain properties of the bulk-ordered alloy, e.g., the valence-band splittings,^{26,27} optical polarization.²⁸ However, it does not give a full account for the absolute energy positions of the valence bands,^{21,29} because the interaction with other bands, especially with the folded band in the $\Gamma-L$ direction, is not taken into account. The interaction with these ignored bands is expected to change when OSL structures are formed. Thus, the current model may not give accurate results for the absolute valence-band positions and the changes in the band gap.

We have used zinc-blende band-edge states as the basis for solving the Hamiltonian of OSL structures. This basis is the same on either side of an OSL interface. What changes as one moves across the interface is the change in the perturbation to the zinc-blende Hamiltonian, which results from the orientational change in the OSL. The justification for this is based on the fact that the VB states for the regions on either side of the interface are constructed from the same set of atomic orbitals. The envelope functions defined in Eq. (8) are continuous at the interfaces, though their derivatives are usually not.

The treatment of the interface in our model is essentially the same as that frequently adopted in conventional superlattices.² The situation in the OSL's is slightly more complex than in conventional superlattices, that is, layers A and B do not have the same microscopic lattice periodicity orientationwise. However, it can be shown in the same way as for conventional superlattices² that to a first-order approximation, the difference in the periodicity has no effect as long as the superlattice period is much larger than the lattice constant. In a more rigorous treatment of the boundary conditions (to a higher-order approximation), the periodicity of the lattice on either side of the interface becomes critical in deriving the boundary conditions for the envelope functions, just as for the conventional superlattices.³⁰ Although the higher-order effects are usually negligible in a conventional superlattice which has a relatively large superlattice period, they could turn out to be more significant in an OSL than in the former. Further consideration of the interface effects is beyond the scope of this work.

B. Orientational superlattices versus conventional superlattices

Superlattice effects in conventional superlattices are usually associated with the discontinuity of energy or effective mass between two layers. By definition, in OSL's, both energy levels and effective masses are identical in the two layers. One would like to ask the following: what is the physical quantity whose discontinuity is the cause of the superlattice effects which appear in OSL's? To answer this question, let us start with Eq. (1), the perturbative Hamiltonian, which brings up all the superlattice effects studied in this work. Note that Eq. (1) has been given in a cubic coordinate system with x , y , and z axes along the $[100]$, $[010]$, and $[001]$ directions, respectively. Assuming layer A orders along the $[111]$ direction, the $[111]$ direction is then a preferred direction for layer A. We can transform Eq. (1) to a coordinate

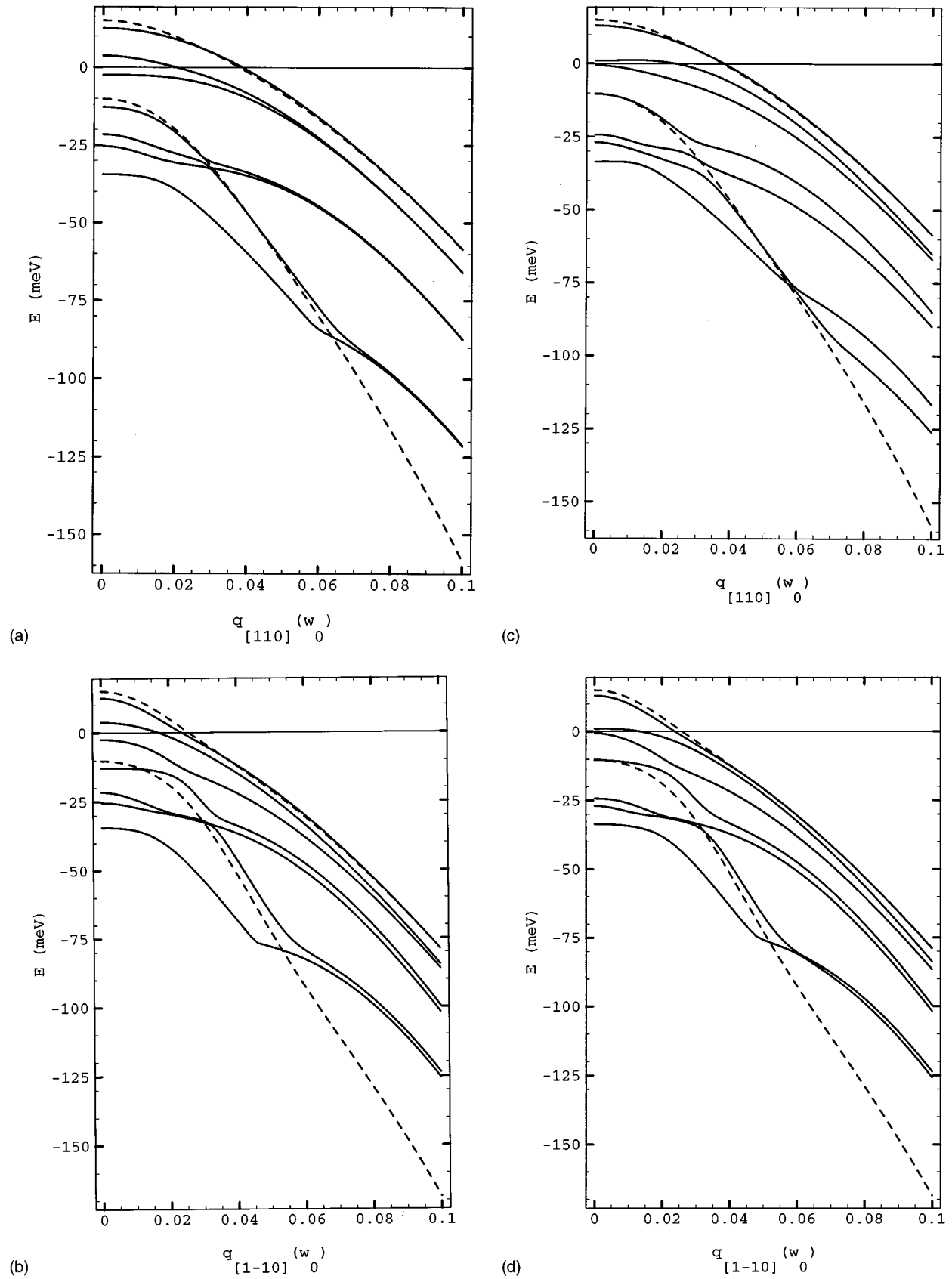


FIG. 8. Energy-dispersion curves of type-I OSL with wave vectors in the plane perpendicular to the superlattice axis: (a) $E(k_{[110]})$ and (b) $E(k_{[1\bar{1}0]})$ for $L_A = L_B = 100 \text{ \AA}$; (c) $E(k_{[110]})$ and (d) $E(k_{[1\bar{1}0]})$ for $L_A = 50 \text{ \AA}$ and $L_B = 150 \text{ \AA}$. Dashed curves are the dispersions for the bulk-ordered alloy in the corresponding directions. $w_0 = 2\pi a$, where a is the lattice constant.

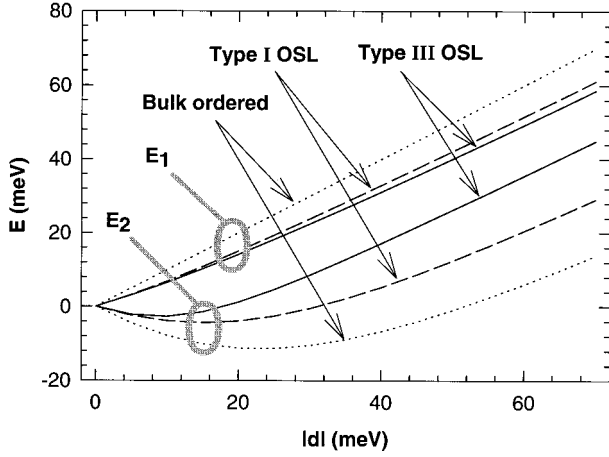


FIG. 9. Energy levels of the first and the second band-edge states as a function of parameter $|d|$ for types-I and -III OSL's with $L_A=L_B=50 \text{ \AA}$, with comparison to the bulk-ordered alloy.

system (x', y', z') , with z' parallel to $[111]$ and y' parallel to $[\bar{1}10]$. In such a coordinate system, the nonzero elements of the tensor ε_A are $\varepsilon_{x'x'} = \varepsilon_{y'y'} = -1$, and $\varepsilon_{z'z'} = 2$, and the perturbation Hamiltonian becomes

$$h(\varepsilon_A) = -d(3L_{z'}^2 - L^2), \quad (10)$$

where $L_{z'}$ is the z' component of angular momentum, and the orientation-dependent term $-3dL_{z'}^2$ makes z' a uniaxis. The rotation R , which transforms region A to B in a SL, changes the tensor ε_A to $\varepsilon_B = R\varepsilon_A R^{-1}$ and the perturbative Hamiltonian $h(\varepsilon_A)$ to $h(\varepsilon_B) = Rh(\varepsilon_A)R^{-1}$. In contrast with the band-offset perturbation of a conventional SL, $h(\varepsilon_B)$ is not diagonal in the $\Gamma_8 \otimes \Gamma_7$ subspace and represents the discontinuity in the angular momentum sensed by an electron moving across the interface. As one can see from Eq. (2), the change in $h(\varepsilon_A)$ brought about by the rotation R directly correlates with the change in ε_A due to the rotation. If \mathbf{u} is a unit vector parallel to the SL-axis, then $\frac{1}{2}(|\varepsilon_A \cdot \mathbf{u}| + |\varepsilon_B \cdot \mathbf{u}|)$ represents the projection of the orientational tensor ε along the SL-axis. Empirically, the confinement energy, i.e., the shift of the topmost VB state, is found to correlate with the quantity $\frac{1}{2}(|\varepsilon_A \cdot \mathbf{u}| + |\varepsilon_B \cdot \mathbf{u}|)$, which is confirmed in Table I. The undulation of the envelope functions can be understood as being the result of interference of Bloch states scattered because of the mismatch of the angular momentum at the interfaces of the orientational domain boundaries.

It is interesting to notice that one cannot make quantum-well structures in the normal sense out of types I–IV OSL's by increasing the thickness of one of the constituents. Only the type-V OSL is similar to a conventional quantum well (the $[111]$ layer is the well, and the $[\bar{1}10]$ layer is the barrier), and to some extent, one can indeed increase the confinement by reducing the well width. However, for types I–IV OSL's one can achieve ground-state confinement in the thicker layer by using the thinner layers as barriers, in contrast with the conventional SL's, where thick barriers are necessary to obtain quantum confinement in the wells. For instance, in a type-I OSL with $L_A=20 \text{ \AA}$ and $L_B=180 \text{ \AA}$, the integrated probability in layer B is greater than 90%, which indicates that a thin layer with one ordering orientation acts as a spacer

between two layers with another ordering orientation. Although for a ground state it is not possible to have the wave function localized in the thinner layer, for certain higher states (for instance, the second states in all the five polytypes), the wave functions can be localized in the thinner layer. This property suggests that it may be possible to generate carriers in alternate layers by tuning the excitation energy.

In this work, we have chosen ordered GaInP₂ alloys as a model system to illustrate the basic properties of orientational superlattices, because the ordering effects are well studied in GaInP₂ alloys. Most calculations are based on the currently obtainable degree of order, which is about 50%. In general, the stronger the ordering or the larger the valence-band splitting, the stronger the OSL effects. It has been demonstrated that many other III-V alloys also showed spontaneous ordering; some of them, in principle, could have larger valence-band splitting than that of the GaInP₂.¹¹ Although the calculations are applied to a specific structure, CuPt-ordered GaInP₂, many qualitative features are applicable, in general, to other possible OSL structures (for instance, CuAu-ordered OSL's, where the ordering directions can be arranged to be perpendicular to each other in the adjacent layers).

Compared to conventional superlattices, the confinement energy is somewhat smaller in OSL's if they have the same layer thickness. For instance, a typical Al_{0.3}Ga_{0.7}As/GaAs superlattice with $L_A=L_B=100 \text{ \AA}$ has a confinement energy of 7.4 meV for the first heavy-hole state. For a type-I OSL with the same layer thickness, the confinement energy will be 2.5 or 4.4 meV for $\sim 50\%$ or 100% -ordered GaInP₂, respectively. One important difference between a conventional superlattice and an OSL is that for a conventional superlattice, the light emitted along the superlattice axis is nearly unpolarized; for an OSL, the emission is strongly polarized, which is a very useful property for a vertical-cavity surface-emitting laser.

IV. SUMMARY AND CONCLUSIONS

We have performed a systematic study on a nonconventional semiconductor heterostructure: orientational superlattices based on CuPt-ordered zinc-blende alloys. Instead of the band offset in conventional superlattices, the discontinuity of the angular momentum is the cause of the superlattice effects in orientational superlattices. Electronic properties of the valence band—energy dispersions, envelope functions, and the probability distributions—for the five polytypes of GaInP₂ OSL's have been classified according to their symmetry and calculated numerically for structures with different periods, ratios of layer thickness, and degree of order. We have shown that wave-function undulation, band-gap modification, and minigaps can be achieved purely from orientational alternation of the semiconductor layers. Features in OSL's similar to those in conventional superlattices are band-gap modification, formation of subbands and minigaps, and wave-function modulation. The distinct properties of OSL's are, for instance, the dependence of energy levels on layer thickness, the wave-function distributions, and strong optical anisotropy. We believe that OSL's are a new field to be explored in semiconductors for both physics and device applications.

ACKNOWLEDGMENTS

We acknowledge S. Froyen's and R. Alonso's involvement in part of this work. We are very grateful for valuable

discussions with A. E. Blakeslee, M. Al-Jassim, S. P. Ahrenkiel, and S.-H. Wei. This work was supported by the Office of Energy Research, Material Science Division of DOE under Contract No. DE-AC36-83CH10093.

-
- ¹L. Esaki and R. Tsu, *IBM J. Res. Dev.* **14**, 61 (1970).
²G. Bastard, *Wave Mechanics Applied to Semiconductor Heterostructures* (Les Editions de Physique, Les Ulis Cedex, 1988).
³A. Mascarenhas, R. G. Alonso, G. S. Horner, and S. Froyen, *Phys. Rev. B* **48**, 4907 (1993).
⁴Yong Zhang, *Phys. Rev. B* **49**, 14 352 (1994).
⁵In the effective-mass lateral SL's, the effective-mass modulation is associated with an inhomogeneously distributed strain, which is similar to the problem of Ref. 4, where the inhomogeneous strain was described by a tensor-type effective potential.
⁶W. H. Backes, P. A. Bobbert, and W. van Haeringen, *Phys. Rev. B* **49**, 7564 (1994).
⁷Z. Ikonc, G. P. Srivastava, and C. J. Inkson, *Phys. Rev. B* **48**, 17 181 (1993).
⁸D. W. Pashley and A. E. B. Presland, *J. Inst. Metals* **87**, 419 (1959).
⁹E. Morita, M. Ikeda, O. Kumagai, and K. Kaneko, *Appl. Phys. Lett.* **53**, 2164 (1988).
¹⁰C. S. Baxter, W. M. Stobbs, and J. H. Wilkie, *J. Cryst. Growth* **112**, 373 (1991).
¹¹A. Zunger and S. Mahajan, in *Handbook on Semiconductors*, 2nd ed., edited by S. Mahajan (Elsevier, Amsterdam, 1994), Vol. 3, Chap. 19, p. 1399.
¹²A. Mascarenhas, Yong Zhang, R. G. Alonso, and S. Froyen, *Solid State Commun.* **100**, 47 (1996).
¹³D. J. Friedman, G. S. Horner, S. R. Kurtz, K. A. Bertness, J. M. Olson, and J. Moreland, *Appl. Phys. Lett.* **65**, 878 (1994).
¹⁴G. S. Chen and G. B. Stringfellow, *Appl. Phys. Lett.* **59**, 324 (1991).
¹⁵Yong Zhang, S. P. Ahrenkiel, and A. Mascarenhas (unpublished).
¹⁶G. P. Srivastava (private communication).
¹⁷P. Bellon, J. P. Chevalier, E. Augarde, J. P. Andre, and G. P. Martin, *J. Appl. Phys.* **66**, 2388 (1989).
¹⁸G. L. Bir and G. E. Pikus, *Symmetry and Strain-Induced Effects in Semiconductors* (Wiley, New York, 1974).
¹⁹F. Pollak, *Surf. Sci.* **37**, 863 (1973).
²⁰S.-H. Wei and A. Zunger, *Phys. Rev. B* **49**, 14 337 (1994).
²¹Yong Zhang and A. Mascarenhas, *Phys. Rev. B* **51**, 13 162 (1995).
²²Coupling with the *L*-valley states might slightly enhance the anisotropic of the conduction band as well as the OSL effects.
²³B. F. Zhu and K. Huang, *Phys. Rev. B* **36**, 8102 (1987); K. Huang, J. B. Xia, B. F. Zhu, and H. Tang, *J. Lumin.* **40/41**, 88 (1988).
²⁴G. A. Baraff and D. Gershoni, *Phys. Rev. B* **43**, 4011 (1991).
²⁵G. Bastard, J. A. Brum and R. Ferreira, in *Solid State Physics*, edited by H. Ehrenreich and D. Turnbull (Academic Press, 1991), Vol. 44, Chap. 2, p. 268.
²⁶P. Ernst, C. Geng, F. Scholz, H. Schweizer, Yong Zhang, and A. Mascarenhas, *Appl. Phys. Lett.* **67**, 2347 (1995).
²⁷Yong Zhang, A. Mascarenhas, P. Ernst, F. A. J. M. Driessen, D. J. Friedman, K. A. Bertness, J. M. Olson, C. Geng, F. Scholz, and H. Schweizer, *J. Appl. Phys.* (to be published).
²⁸B. Fluegel, Yong Zhang, H. M. Cheong, A. Mascarenhas, J. Geisz, J. M. Olson, and A. Duda, *Phys. Rev. B* (to be published).
²⁹S. Froyen, A. Zunger, and A. Mascarenhas, *Appl. Phys. Lett.* **68**, 2852 (1996).
³⁰M. G. Burt, *J. Phys. Condens. Matter* **4**, 6651 (1992).